

Configurational statistics of densely and fully packed loops in the negative-weight percolation model

O. Melchert and A. K. Hartmann

Institut für Physik, Universität Oldenburg, Carl-von-Ossietzky Strasse, 26111 Oldenburg, Germany

Received: date / Revised version: date

Abstract. By means of numerical simulations we investigate the configurational properties of densely and fully packed configurations of loops in the negative-weight percolation (NWP) model. In the presented study we consider $2d$ square, $2d$ honeycomb, $3d$ simple cubic and $4d$ hypercubic lattice graphs, where edge weights are drawn from a Gaussian distribution. For a given realization of the disorder we then compute a configuration of loops, such that the configurational energy, given by the sum of all individual loop weights, is minimized. For this purpose, we employ a mapping of the NWP model to the “minimum-weight perfect matching problem” that can be solved exactly by using sophisticated polynomial-time matching algorithms. We characterize the loops via observables similar to those used in percolation studies and perform finite-size scaling analyses, up to side length $L = 256$ in $2d$, $L = 48$ in $3d$ and $L = 20$ in $4d$ (for which we study only some observables), in order to estimate geometric exponents that characterize the configurations of densely and fully packed loops. One major result is that the loops behave like uncorrelated random walks from dimension $d = 3$ on, in contrast to the previously studied behavior at the percolation threshold, where random-walk behavior is obtained for $d \geq 6$.

1 Introduction

The statistical properties of lattice-path models on graphs, equipped with quenched disorder, have experienced much attention during the last decades. They have proven to be useful in order to describe line-like quantities as, e.g., linear polymers in disordered media [1,2,3,4], vortices in high T_c superconductivity [5,6], cosmic strings in the early universe [7,8,9], and domain-wall excitations in disordered media such as $2d$ spin glasses [10,11] and the $2d$ solid-on-solid model [12]. The precise computation of these paths can often be formulated in terms of a combinatorial optimization problem and hence might allow for the application of exact optimization algorithms developed in computer science [13,14,15]. So as to analyze the statistical properties of these lattice path models, geometric observables and scaling concepts similar to those used in percolation theory [16,17] or other “string”-bearing models [18,19] are often applicable.

The topic of the presented article is the *negative-weight percolation* (NWP) problem [20,21,22], wherein one considers a regular lattice graph with periodic boundary conditions (BCs) and where adjacent sites are joined by undirected edges. Weights are assigned to the edges, representing quenched random variables drawn from a distribution that allows for edge weights of either sign. For a given realization of the disorder, one then computes a configuration of loops, i.e. closed paths on the lattice graph, such that the total sum of the weights assigned to the edges that build up the loops attains an *exact* minimum. Note that

the application of exact algorithms in contrast to standard sampling approaches like Monte Carlo simulations avoids, e.g., equilibration problems. Also, since the algorithms run in polynomial time, large instances can be solved. As an additional optimization constraint we impose the condition that the loops are not allowed to intersect. Consequently, since a loop does neither intersect with itself nor with other loops in its neighborhood, it exhibits an “excluded volume” quite similar to usual self avoiding walks (SAWs) [17]. The problem of finding these loops can be cast into a minimum-weight path (MWP) problem, outlined below in sect. 2 in more detail.

In previous studies [20,21,22], the details of the weight distribution were further controlled by a tunable disorder parameter. As a pivotal observation it was found that, as a function of the disorder parameter, the NWP model features a disorder driven, geometric phase transition. This transition leads from a phase characterized by only “small” loops to a phase that also features “large” loops that span the entire lattice along at least one direction. Regarding these two phases and in the limit of large system sizes, there is a particular value of the disorder parameter at which percolating (i.e. system spanning) loops appear for the first time [20]. Previously, we have investigated the NWP phenomenon for $2d$ lattice graphs [20] using finite-size scaling (FSS) analyses, where we characterized the underlying transition by means of a whole set of critical exponents. Considering different disorder distributions and lattice geometries, the exponents were found to be universal in $2d$ and clearly distinct from those

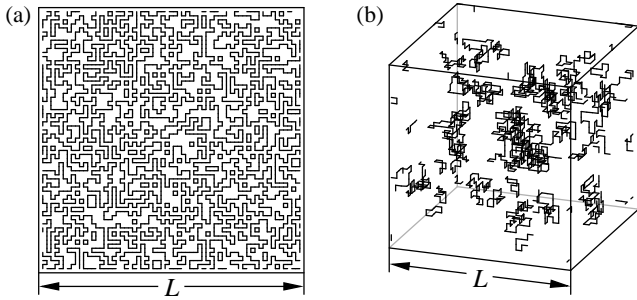


Fig. 1. Illustration of densely packed loop (DPL) configurations. (a) Sample configuration of DPLs for a square lattice of side length $L = 64$ and fully periodic boundary conditions (BCs), and (b) configuration of DPLs for a simple cubic lattice of side length $L = 32$ and fully periodic BCs. For a more clear presentation, small loops with length $\ell < 10$ and a very large loop with length $\ell = 26\,770$ were omitted from the latter figure.

describing other percolation phenomena. In a subsequent study we investigated the effect of dilution on the critical properties of the $2d$ NWP phenomenon [21]. Therefore we performed FSS analyses to probe critical points along the critical line in the disorder-dilution plane that separates domains that allow/disallow system spanning loops. One conclusion of that study was that bond dilution changes the universality class of the NWP problem. Further we found that, for bond-diluted lattices prepared at the percolation threshold of $2d$ random percolation and for purely Gaussian distributed edge-weights, the geometric properties of the system spanning loops compare well to those of ordinary self-avoiding walks. Lately, we performed further simulations for the NWP model on hypercubic lattice graphs in dimensions $d = 2$ through 7 [22], where we found evidence for an upper critical dimension $d_u = 6$ of the NWP phenomenon. To resume, up to now we have focused on the critical properties of the NWP model in the vicinity of the critical point at which percolating loops first appear in the limit of large system sizes. As we experienced, at this critical point the loops are rather isolated and well separated from each other, i.e. they resemble a dilute gas of loops. However, as the disorder on the lattice increases, the loops get more dense and it is reasonable to ask for the statistical properties of these densely packed configurations of loops.

Here, we investigate the NWP model on $2d$ square and honeycomb, $3d$ simple cubic and $4d$ hypercubic lattice graphs for a purely Gaussian distribution of the edge weights. Therein, our aim is to characterize the minimum-weight configurations of densely packed loops (DPLs), see Fig. 1, regarding their statistical properties. Further, we present a modification of the NWP algorithm that allows for the computation of configurations of fully packed loops (FPLs). Regarding a configuration of FPLs, each site on the lattice is visited by a loop. We find that the scaling properties of DPLs and FPLs for the $2d$ systems agree within errorbars and compare well to those obtained for FPLs related to other discrete interface models [23]. Fur-

ther, the geometric properties of the loops for $3d$ systems are similar to those of completely uncorrelated random walks, indicating that the upper critical dimension shifts to $d_u^{\text{DPL}} = 3$ for DPLs.

The remainder of the presented article is organized as follows. In section 2, we introduce the model in more detail and we outline the algorithm used to compute the minimum weight configurations of loops (i.e. DPLs and FPLs). In section 3, we present the results of our numerical simulations and in section 4 we conclude with a summary.

2 Model and Algorithm

In the remainder of this article we consider regular $2d$ square/honeycomb, $3d$ simple cubic and $4d$ hypercubic lattice graphs $G = (V, E)$ with side length L and fully periodic boundary conditions (BCs). The considered graphs have $N = |V| = L^d$ sites $i \in V$ and a number of $|E| = zN/2$ undirected edges $\{i, j\} \in E$ that join adjacent sites $i, j \in V$. Above, z signifies the coordination number of the lattice geometry, where $z = 4, 3, 6$ and 8 for square, honeycomb, simple cubic and $4d$ hypercubic lattice graphs, respectively. We further assign a weight ω_{ij} to each edge contained in E . These weights represent quenched random variables that introduce disorder to the lattice. In the presented article we consider independent identically distributed weights drawn from a Gaussian disorder distribution with mean zero and unit width, i.e.

$$P(\omega) = \exp(-\omega^2/2)/\sqrt{2\pi}. \quad (1)$$

Note that this distribution explicitly allows for loops \mathcal{L} with a negative total weight $\omega_{\mathcal{L}} = \sum_{\{i,j\} \in \mathcal{L}} \omega_{ij}$. So as to support intuition: Eq. 1 corresponds to the limit $\rho = 1$ of the disorder parameter for the edge-weight distribution considered in previous studies of the NWP model, see e.g. Ref. [22]. Accordingly, we here consider the NWP phenomenon high up in the percolating phase where the minimal weight configurations of loops are densely packed.

The NWP problem then reads as follows: Given G together with a realization of the disorder, determine a set \mathcal{C} of loops such that the configurational energy, defined as the sum of all the loop-weights $\mathcal{E} = \sum_{\mathcal{L} \in \mathcal{C}} \omega_{\mathcal{L}}$, is minimized. As further optimization constraint, the loops are not allowed to intersect. Clearly, the configurational energy \mathcal{E} is the quantity subject to optimization and the result of the optimization procedure is a set of loops \mathcal{C} , obtained using an appropriate transformation of the original graph as detailed in [24]. For the transformed graphs, *minimum-weight perfect matchings* (MWPMs) [25,26,27] are calculated, that serve to identify the loops for a given realization of the disorder. This procedure allows for an efficient implementation [28] of the simulation algorithms. Until further notice, the subsequent description applies to DPLs only. In order to obtain FPLs, the transformation is slightly different (see discussion below). Here, we give a brief description of the algorithmic procedure that yields a minimum-weight set of loops for a given realization of

the disorder. Fig. 2 illustrates the 3 basic steps, detailed below:

(1) each edge, joining adjacent sites on the original graph G , is replaced by a path of 3 edges. Therefore, 2 “additional” sites have to be introduced for each edge in E . Therein, one of the two edges connecting an additional site to an original site gets the same weight as the corresponding edge in G . The remaining two edges get zero weight. The original sites $i \in V$ are then “duplicated”, i.e. $i \rightarrow i_1, i_2$, along with all their incident edges and the corresponding weights. For each of these pairs of duplicated sites, one additional edge $\{i_1, i_2\}$ with zero weight is added that connects the two sites i_1 and i_2 . The resulting auxiliary graph $G_A = (V_A, E_A)$ is shown in Fig. 2(b), where additional sites appear as squares and duplicated sites as circles. Fig. 2(b) also illustrates the weight assignment on the transformed graph G_A . Note that while the original graph (Fig. 2(a)) is symmetric, the transformed graph (Fig. 2(b)) is not. This is due to the details of the mapping procedure and the particular weight assignment we have chosen. A more extensive description of the mapping can be found in [11].

(2) a MWPM on the auxiliary graph is determined via exact combinatorial optimization algorithms [29]. A MWPM is a minimum-weighted subset M of E_A , such that each site contained in V_A is met by precisely one edge in M . This is illustrated in Fig. 2(c), where the solid edges represent M for the given weight assignment. The dashed edges are not matched. Due to construction, the auxiliary graph consists of an even number of sites and the transformation procedure described in step (1) guarantees that a perfect matching exists. Note that a MWPM can be computed in polynomial time as a function of the number of sites, hence large systems with several thousands of sites are feasible.

(3) finally it is possible to find a relation between the matched edges M on G_A and a configuration of negative-weighted loops \mathcal{C} on G by tracing back the steps of the transformation (1). As regards this, note that each edge contained in M that connects an additional site (square) to a duplicated site (circle) corresponds to an edge on G that is part of a loop, see Fig. 2(d). Note that, by construction of the auxiliary graph, for each site i_1 or i_2 matched in this way, the corresponding twin site i_2/i_1 must be matched to an additional site as well. This guarantees that wherever a path enters a site of the original graph, the paths also leaves the site, corresponding to the defining condition of loops. All the edges in M that connect like sites (i.e. duplicated-duplicated, or additional-additional) carry zero weight and do not contribute to a loop on G . Once all loop segments are found, a depth-first search [24,26] can be used to identify the loop set \mathcal{C} and to determine the geometric properties of the individual loops. Here, the exemplary weight assignment illustrated in Fig. 2(a) yields 2 loops, i.e. $\mathcal{C} = \{\mathcal{L}_1, \mathcal{L}_2\}$, with weights $\omega_{\mathcal{L}_1} = \omega_{\mathcal{L}_2} = -4$ and lengths $\ell_1 = \sum_{\{i,j\} \in \mathcal{L}_1} 1 = 8$, $\ell_2 = 4$. Hence, the configurational energy reads $\mathcal{E} = -8$.

The result of the calculation is a collection \mathcal{C} of loops such that the total loop weight, and consequently the con-

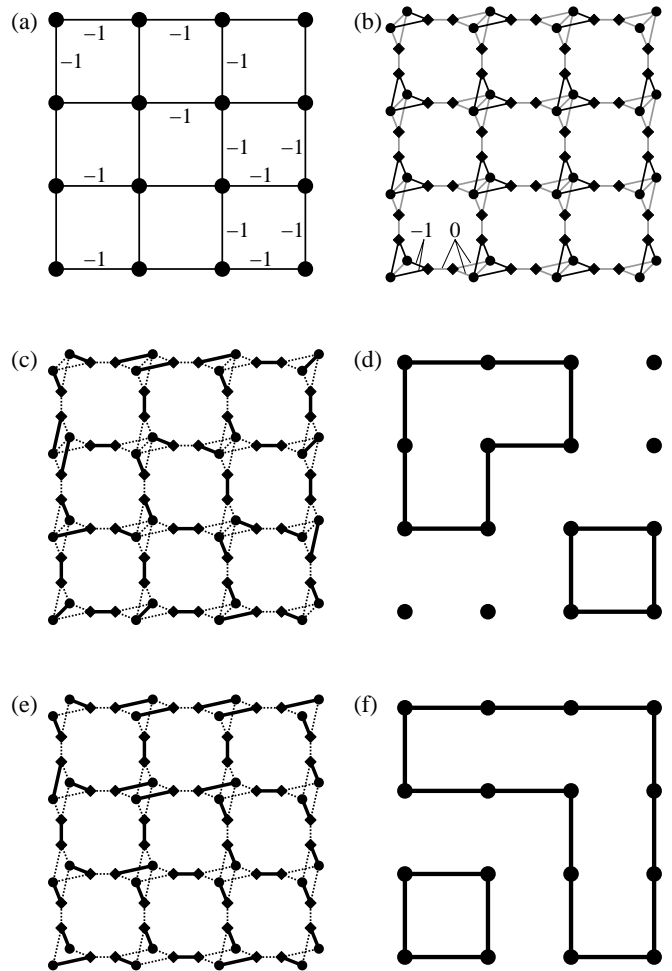


Fig. 2. Illustration of the algorithmic procedure: (a) original lattice G with edge weights. For clarity, a bimodal distribution that yields edge-weights ± 1 is considered. Further, only negative edge-weights are shown. Unlabeled edges have weight $+1$. (b) auxiliary graph G_A with proper weight assignment. Black edges carry the same weight as the respective edge in the original graph and gray edges carry zero weight, (c) minimum-weight perfect matching (MWPM) M : bold edges are matched and dashed edges are unmatched, and (d) loop configuration (bold edges) that corresponds to the MWPM depicted in (c). (e) MWPM for the the modified mapping that yields fully packed configurations of loops. (f) fully packed loops (bold edges) that correspond to the MWPM shown in (e).

figurational energy \mathcal{E} , is minimized. Hence, one obtains a global collective optimum of the system. Obviously, all loops that contribute to \mathcal{C} possess a negative weight. Also note that the choice of the weight assignment in step (1) is not unique, i.e. there are different possibilities to choose a weight assignment that all result in equivalent sets of matched edges on the transformed lattice, corresponding to the minimum-weight collection of loops on the original lattice. Some of these weight assignments result in a more symmetric transformed graph, see e.g. [24]. However, this

is only a technical issue that does not affect the resulting loop configuration. Finally, for an illustrational purpose, a small $2d$ lattice graph with free BCs was chosen intentionally. The algorithmic procedure extends to higher dimensions and fully periodic BCs in a straight-forward manner.

Note that, by means of the algorithmic procedure outlined above, its also possible to compute configurations of fully packed loops. To accomplish this, only one detail related to step (1) has to be altered. I.e., original sites $i \in V$ are duplicated ($i \rightarrow i_1, i_2$) to yield $i_1, i_2 \in V_A$, but *no* additional edge $\{i_1, i_2\}$ is added to E_A . By construction, a MWPM, as computed in step (2), will not contain an edge that connects a tuple of duplicated sites (since there are no such edges present). Hence, in the resulting MWPM, each duplicated site will be matched to an additional site, see Fig. 2(e). Applying step (3), one then finds that a each site on the original graph is an endpoint of exactly two loop segments, see Fig. 2(f), and the result is a fully packed configuration of loops. Applying this modified mapping to the exemplary weight assignment illustrated in Fig. 2(a) yields $\mathcal{C}_{\text{FPL}} = \{\mathcal{L}_1, \mathcal{L}_2\}$ (see Fig. 2(f)), with weights $\omega_{\mathcal{L}_1} = -6$, $\omega_{\mathcal{L}_2} = 0$ and lengths $\ell_1 = 12$, $\ell_2 = 4$. Here, the configurational energy reads $\mathcal{E} = -6$.

Apparently, there are qualitative differences between configurations of DPLs and FPLs: Regarding the DPLs, not all lattice sites are visited by a loop (see Fig. 1(a)), and, due to the “energy minimization principle” of the optimization procedure, the weight of an individual loop is strictly smaller than zero. In contrast, FPLs require each lattice site to be visited by a loop. This constitutes a “hard” constraint for the optimization procedure and as a result, an individual loop weight might take a value larger than or equal to zero (as for the assignment of ± 1 edgeweights in Fig. 2(a)).

Subsequently, we will use the procedure outlined above so as to investigate the NWP model on $2d$ square and honeycomb and $3d$ simple cubic lattice graphs with a Gaussian distribution of edge weights.

3 Results

In order to characterize the statistical properties of configurations of DPLs we performed simulations for $2d$ square ($2d$ -sq) systems with a linear extension of up to $L = 256$ lattice sites, and $3d$ simple cubic ($3d$ -sc) systems with side length up to $L = 48$ sites. If not stated explicitly, the results presented in the remainder of this section follow from an analysis of the full ensemble of loops obtained for a fixed system size, i.e. $L = 256$ (48) in $2d$ ($3d$). For both setups we considered a number of $n = 12800$ independent realizations of the disorder to compute averages. Moreover, we conducted simulations for a $2d$ honeycomb ($2d$ -hy) DPL and $2d$ -sq FPL version of the loop model for lattices up to $L = 128$, where we considered $n = 9600$ samples for the largest systems. We performed additional simulations for $4d$ hypercubic ($4d$ -hc) lattice graphs with $L = 20$ and $n = 9600$ in order to study selected observables for an even higher dimension.

Next, we briefly introduce the basic observables we used to characterize the individual loops obtained from the simulations. As introduced earlier, two fundamental quantities related to a given loop are its weight $\omega_{\mathcal{L}}$ and length ℓ . We further determine the linear extensions R_i , $i = 1 \dots d$, of each loop by projecting it onto the independent lattice axes (for the hexagonal lattice geometry we therefore use the topologically equivalent brickwall lattice). The largest of those values, i.e.

$$R = \max_{i=1 \dots d} (R_i), \quad (2)$$

is referred to as the *spanning length* of the loop and the smallest, i.e.

$$r = \min_{i=1 \dots d} (R_i), \quad (3)$$

is called its *roughness*. Moreover, so as to characterize the full perimeter of an individual loop on a coarse grained scale, we can define the *size*

$$R_s = \sum_{i=1}^d R_i, \quad (4)$$

i.e. the length of the loop if all small scale irregularities were flattened [7]. Note that the linear extensions of a given loop are measured in units of lattice sites. E.g., the loop \mathcal{L}_1 contained in the example illustrated in Fig. 2(d) has $R_1 = R_2 = 3$ and thus $R_s = 6$. Albeit this definition of a loop size is somewhat odd for small loops in a $3d$ setup (where an elementary loop of length $\ell = 4$ has size $R_s = 5$, as noted in Ref. [7]), it nevertheless gives a reasonable definition of a coarse grained loop size in the limit of large ℓ . Anyway, note that there are some difficulties related to the “extremal” loops on the lattice. This means, if we consider the full ensemble of loops for a system of size L , there are very small loops ($R \ll L$) which are affected by the finite lattice spacing and also very large loops ($R \approx L$) that are affected by the finite size of the considered system. So as to obtain most reliable estimates for the observables that characterize the configurations of loops, and if not stated explicitly, these extremal loops are discarded from the analysis. Subsequently, we will adopt the notation $\langle O \rangle$ to signify the disorder averaged value of observable O . Whenever a more clear presentation requires, we will write $\langle O \rangle_X$ to signify the disorder averaged value of O with respect to the quantity X .

In the following we will present the results on the geometric properties of the DPL/FPL configurations in subsection 3.1, the results on the energetic properties are summarized in subsection 3.2.

3.1 Geometric properties

As pointed out above, we here report our results regarding the geometric properties of the loop configurations obtained for the $2d$ ($3d$, $4d$) systems mention in the beginning of the presented section.

Table 1. “Packing” properties, scaling exponents and parameters that characterize DPLs/FPLs on the considered lattice graphs. From left to right: System setup [sq=square, hy=honeycomb, sc=simple cubic, hc=hypercubic; DPLs (FPLs)=densely (fully) packed loops], linear extension L of the lattice for which the listed estimates were obtained, number n of samples considered, approximate number N_{loops} of loops collected during the simulations, probability ρ_{cov} that a lattice site is visited by a loop, fraction f_{∞} of loop segments contained in system spanning loops and “loop-shape” parameter $a/(2d^2)$. Fractal dimension d_f , correction to scaling exponent ω and exponent τ that describe the scaling of the non-spanning loops. Scaling dimension d'_f for the largest loops found for each realization of the disorder and asymptotic estimate ϵ for the normalized configurational weight.

		L	n	N_{loops}	ρ_{cov}	f_{∞}	$a/(2d^2)$	d_f	ω	τ	d'_f	$\langle \epsilon \rangle$
2d-sq	DPLs	256	12 800	25×10^6	0.825	0.327	0.97(3)	1.756(8)	0.86(8)	2.14(2)	1.752(1)	0.596
2d-sq	FPLs	128	9 600	6×10^6	1.000	0.371	0.98(1)	1.75(2)	0.9(2)	2.16(1)	1.751(1)	0.493
2d-hy	DPLs	128	9 600	2×10^6	0.750	0.429	1.04(4)	1.75(2)	1.0(1)	2.14(1)	1.750(1)	0.412
3d-sc	DPLs	48	12 800	13×10^6	0.901	0.907	0.96(1)	2.01(4)	0.66(11)	2.49(6)	3.00(1)	0.844
4d-hc	DPLs	20	9 600	6×10^6	0.938	0.970	0.99(3)	2.00(5)	-	-	-	1.013

Global “packing” properties: As pointed out above, for the configurations of DPLs considered here, not all lattice sites are visited by a loop. We can quantify this by computing the probability ρ_{cov} that some site on the lattice lies on the perimeter of a loop, see Tab. 1. Via additional simulations for other system sizes (not shown here), we verified that the value of ρ_{cov} is basically independent of the lattice sizes. From the accumulated data we also obtained the probability ρ_{∞} that some site on the lattice lies on the perimeter of a large, i.e. system spanning, loop. From this we conclude that a fraction $f_{\infty} \equiv \rho_{\infty}/\rho_{\text{cov}}$ (see Tab. 1) of all loop segments for the 2d-sq, 2d-hy, 3d-sc and 4d-hc setup is contained in large loops. Further, note that the estimate $f_{\infty} \approx 0.371$ for the 2d-sq FPL version of the loop model (where $\rho_{\text{cov}} = 1$, exactly) is somewhat larger than the corresponding value $f_{\infty} \approx 0.327$ for the DPL configurations. As evident by comparing the estimates ρ_{cov} and f_{∞} obtained for DPLs on 2d square and honeycomb lattice graphs, the observables above characterize the particular lattice geometries chosen and hence are not universal.

Scaling of the loop shape: Next, we want to study the scaling behavior of the average loop shape. As in Refs. [7,22] we therefore monitor the volume to surface ratio $V_{\text{B}}/S_{\text{B}}$ of the smallest box that fits the individual loops as a function of the coarse-grained loop size R_s , where $V_{\text{B}} = \prod_{i=1}^d R_i$ and $S_{\text{B}} = 2 \times \sum_{i=1}^d V_{\text{B}}/R_i$. For hypercubic volumes with identical values $R_1 = \dots = R_d$, one would expect to find $V_{\text{B}}/S_{\text{B}} = (2d^2)^{-1} R_s$. Performing fits to the form $\langle V_{\text{B}}/S_{\text{B}} \rangle = a R_s^{\psi}$, discarding very small and large non-percolating loops, we here yield the results $\psi = 1.002(5)$ (1.001(1)) and $a = 0.121(3)$ (0.0535(3)) that describe 2d-sq (3d-sc) configurations of DPLs. Further, for the 2d-sq FPL data we obtain $\psi = 0.999(2)$ and $a = 0.123(1)$. For the 2d-hy setup our data is consistent with the precise scaling expression $\langle V_{\text{B}}/S_{\text{B}} \rangle = 0.130(5)(R_s - 0.4)^{1.006(8)}$, that includes corrections to scaling in a very basic form. The same holds also for the 4d-hc setup, where $\langle V_{\text{B}}/S_{\text{B}} \rangle = 0.031(1)(R_s - 0.5)^{0.994(8)}$. Hence, we find values of $a/(2d^2)$ (see Tab. 1) reasonably close to 1 in order to conclude that,

in a statistical sense, the loops are not oblate but possess a rather spherical shape.

Scaling of the loop length – “small” loops: The geometric properties of the loops can further be characterized by the fractal dimension d_f . It can be defined from the scaling of the average loop length $\langle \ell \rangle$ as a function of the loop size according to $d_f = \lim_{R_s \rightarrow \infty} \log(\langle \ell \rangle) / \log(R_s)$. Lower and upper bounds on the above estimate of d_f can be obtained in a systematic way [30]: Based on the expression $R_s = \sum_{i=1}^d R_i$ for the loop size, it is intuitive that $R_s^- = d \cdot r$ typically underestimates the value of R_s (bear in mind that $r = \min_{i=1\dots d}(R_i)$). Consequently, the scaling assumption $\langle \ell \rangle_r \sim r^{d_f^-}$ yields an estimate $d_f^- \leq d_f$. In the same sense, $R_s^+ = d \cdot R$ overestimates R_s and gives rise to a scaling exponent $d_f^+ \geq d_f$. However, in the limit of large loops and since the loops have rather spherical shape (which implies $r \approx R$), we should be able to verify $d_f^- = d_f = d_f^+$. For the 2d and 3d systems considered, we found our data best fit by a scaling function that includes corrections to scaling in the form $\langle \ell \rangle \sim X^{d_f}(1 + cX^{-\omega})$, where X optionally stands for r , R_s or R . In this regard we yield the estimates listed in Tab. 2 and fit-parameters c of the order of unity (Note that for the 4d hypercube with $L = 20$, since the range of values for the scaling parameters r and R is too small, our data did not allow for a decent analysis of upper and lower bounds). The exponents for the choice $X = R_s$ are listed in Tab. 1 and the data for the 2d-sq (3d-sc) DPLs is shown in Fig. 3. When comparing the resulting estimates of $d_f^{+/-}$ and d_f , keep in mind that the presence of corrections to scaling hinders the straight forward fit to a pure power law function. As an alternative to the scaling function considered above, one might choose a more basic expression that accounts for corrections to scaling and features less free parameters. In this regard, for the 2d-sq FPL setup we obtained $\langle \ell \rangle \sim (R_s + 1.5(4))^{1.747(9)}$, in agreement with the estimate listed in Tab. 1. From the simulations for the 4d systems and in the limit of large loops, we found a good fit of

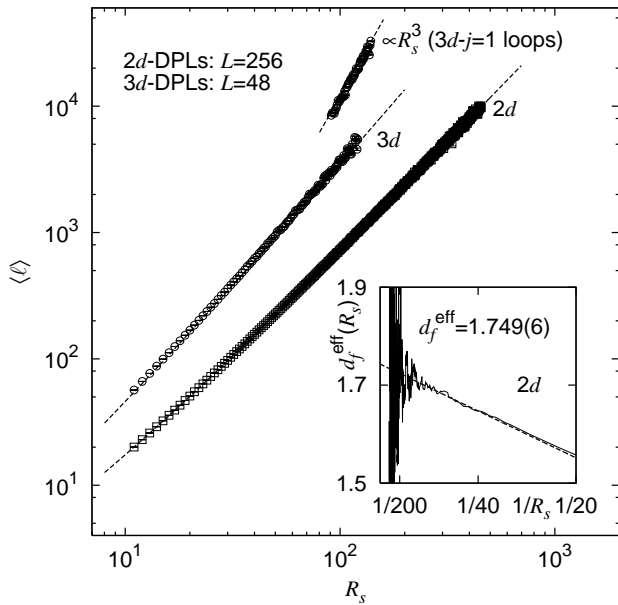


Fig. 3. Scaling of the average loop length $\langle \ell \rangle$ of the non-spanning DPLs as a function of the coarse grained loop size R_s for $2d$ square and $3d$ simple cubic lattice graphs (the $3d$ data is shifted upwards by a factor of 3). Further, the upmost data curve indicates the scaling $\sim R_s^3$ of $3d$ loops with spanning index $j=1$, i.e. those loops that span the system along exactly one direction (the respective data points are shifted upwards by a factor of 12). The inset illustrates the sequence of effective scaling exponents d_f^{eff} as function of the inverse loop size for the DPL setup on the $2d$ square lattice.

the data to the form $\langle \ell \rangle \sim R_s^{d_f}$, resulting in the estimate $d_f = 2.00(5)$.

As further check of the results for the $2d$ -sq ($3d$ -sc) DPLs obtained above, we computed the effective (local) slopes that describe the scaling of $\langle \ell \rangle$ within intervals of, say, m consecutive data points R_s according to $\log(\langle \ell \rangle) = d_f^{\text{eff}} \log(R_s) + c$. By sliding this “scaling window” over the whole data set, one obtains a sequence of

Table 2. Extended analysis of scaling exponents and parameters that characterize DPLs/FPLs. From left to right: lattice setup [sq=square, hy=honeycomb, sc=simple cubic; DPLs (FPLs) = densely (fully) packed loops], lower and upper bounds $d_f^{-/+}$ on the fractal dimension and corresponding correction to scaling exponents $\omega^{+/-}$ that describe the scaling of the non-spanning loops as explained in the text.

		d_f^-	ω^-	d_f^+	ω^+
2d-sq	DPLs	1.749(6)	0.8(3)	1.751(5)	0.92(5)
2d-sq	FPLs	1.73(2)	1.1(3)	1.75(1)	0.7(1)
2d-hy	DPLs	1.73(4)	1.0(3)	1.75(2)	1.1(1)
3d-sc	DPLs	2.0(1)	0.5(2)	2.0(3)	0.3(4)

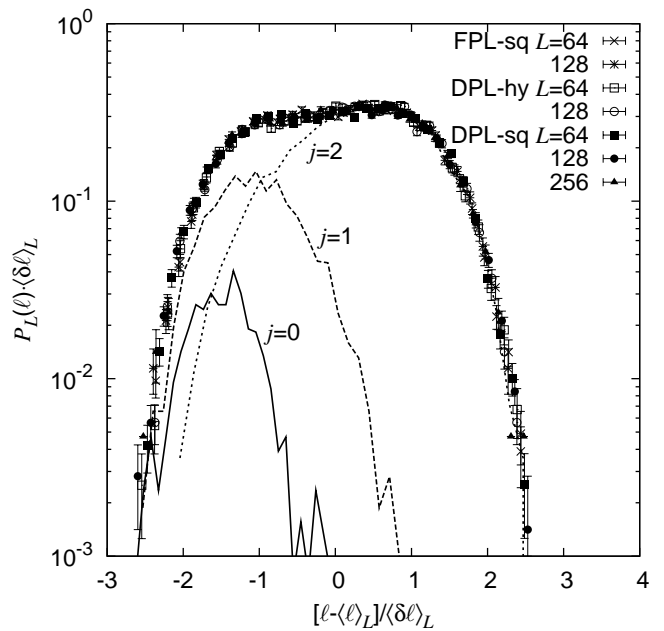


Fig. 4. Scaling behavior of the probability density function $P_L(\ell)$ of the loop length ℓ , considering the largest loop found for each realization of the disorder for different system sizes L . After rescaling, data curves for the different $2d$ setups [DPLs (FPLs) = densely (fully) packed loops; sq=square, hy=honeycomb] fall onto one universal scaling function. Further, the contribution of the loops with spanning index $j=0, 1, 2$ (see text) to the $L=256$ ($2d$ DPL-sq) data curve is illustrated.

effective exponents $d_f^{\text{eff}}(R_s)$. The asymptotic value d_f^{eff} is then extrapolated by means of a straight line fit to the plot of $d_f^{\text{eff}}(R_s)$ as a function of the inverse loop size. For the $2d$ -sq ($3d$ -sc) DPL data, setting $m=20$ (10), this procedure yields the estimates $d_f^{\text{eff}} = 1.749(6)$ ($1.98(3)$), that agree with those listed in Tab. 1 within errorbars. The results for the DPLs on the $2d$ square lattice are further shown in the inset of Fig. 3.

Referring to the numerical values of d_f found here, and from a point of view of statistical physics, the loops appear to be self similar fractals. Albeit the loops are self avoiding by construction, our results indicate that for $d \geq 3$ they exhibit the statistical properties of completely uncorrelated random curves with $d_f = 2$. Hence, this suggests that the upper critical dimension of the NWP problem in the limit of DPLs is $d_u^{\text{DPL}} = 3$.

Scaling of the loop length – “large” loops: So far, the data analyses referred to the subset of non-spanning loops found for the simulated disorder samples. However, as discussed above, about 91% of the over all loop length for the $3d$ -sc systems is contained in very large, i.e. system spanning, loops (see Tab. 1). For this setup we further observe that, in comparison to the small loops investigated above, very large system spanning loops exhibit different scaling properties. These loops are a direct consequence

of the periodic boundary conditions, and, although they are strongly affected by the finite size of the “simulation box”, we might nevertheless characterize their configurational properties.

To perform a systematic analysis of these very large loops, we here introduce the spanning index $j \in \{0 \dots d\}$ of an individual loop. As regards this, a value of, say, $j = 2$ indicates that the respective loop spans the lattice along exactly 2 of the d independent lattice directions (non-spanning loops have $j = 0$). Note that for a single configuration of the disorder, the number of loops having $j \geq 1$ is rather small. E.g., simulating $n = 12\,800$ instances for a $3d$ simple cubic system with $L = 48$ we count $N_{\text{loops}}^j = 4\,149, 3\,260, 31\,106$ for $j = 1, 2, 3$, respectively (for comparison $N_{\text{loops}}^{j=0} = 13\,665\,016$). Hence, the results below should be recognized as “guiding values” that are to be encountered with some caution.

Now, filtering the $3d$ data for loops with spanning index $j = 1$, we observe a power law scaling of the form $\langle \ell \rangle \sim R_s^{3.0(1)}$, see Fig. 3. Considering a loop with spanning index $j = 2$, one might argue that the roughness r is a more adequate scaling variable. Note that for loops with $j = 2$ on a lattice of side length $L = 48$ one has $r = R_s - 2 \cdot 48$. As regards this, upon analysis we find a best fit of the data to the form $\langle \ell \rangle \sim (R_s - 91(8))^{1.7(3)}$. However, as mentioned above, the number of loops having $j = 2$ is rather small. Hence the statistics for these loops is rather poor and the above estimate presents only an approximate result. Note that no such scaling analysis is possible for a spanning index $j = d$, since the corresponding loops all have $R_s = d \cdot L$.

Regarding the $4d$ data we yield $N_{\text{loops}}^j = 6625020, 2873, 1\,939, 2\,021$ and $30\,961$ for $j = 0, \dots, 4$, respectively. Due to the small number of loops having $j = 1, 2, 3$, no decent scaling analysis was possible.

We also performed FSS analyses according to $\langle \ell \rangle \sim L^{d'_f}$, where, for different system sizes L , we consider only the largest loop found for each realization of the disorder. In this regard we were able to verify the “small loop” scaling behavior for the $2d$ systems, i.e. $d'_f \approx 1.75$, see Tab. 1. A similar scaling analysis for the $3d$ -sc data yields $\langle \ell \rangle \sim L^{3.00(1)}$ (not shown), where all loops considered (i.e. the largest loop for each realization of the disorder) turned out to have $j = 3$. In $4d$ we performed simulations for $L = 20$ only. Hence no such scaling analysis is carried out for the $4d$ setup.

The probability density function (pdf) $P_L(\ell)$ of the length ℓ for the largest loop for a given realization of the disorder is shown in Fig. 4. As evident from the figure, the data for all the $2d$ setups considered fall onto one master curve, if rescaled according to $P_L(\ell) = \langle \delta \ell \rangle_L^{-1} p_0[(\ell - \langle \ell \rangle_L) / \langle \delta \ell \rangle_L]$. Therein, $p_0[\cdot]$ signifies a scaling function and $\langle \delta \ell \rangle_L = [(\langle \ell^2 \rangle_L - \langle \ell \rangle_L^2)]^{1/2}$ refers to the root mean square deviation related to the loop length ℓ . This data collapse highlights that the different geometries and types of loops exhibit an universal behavior. We further observed that each data curve is composed of three parts that relate to loops with different values of j . For the $2d$ DPLs on the $L = 256$ square lattice, Fig. 4 also shows the contribution

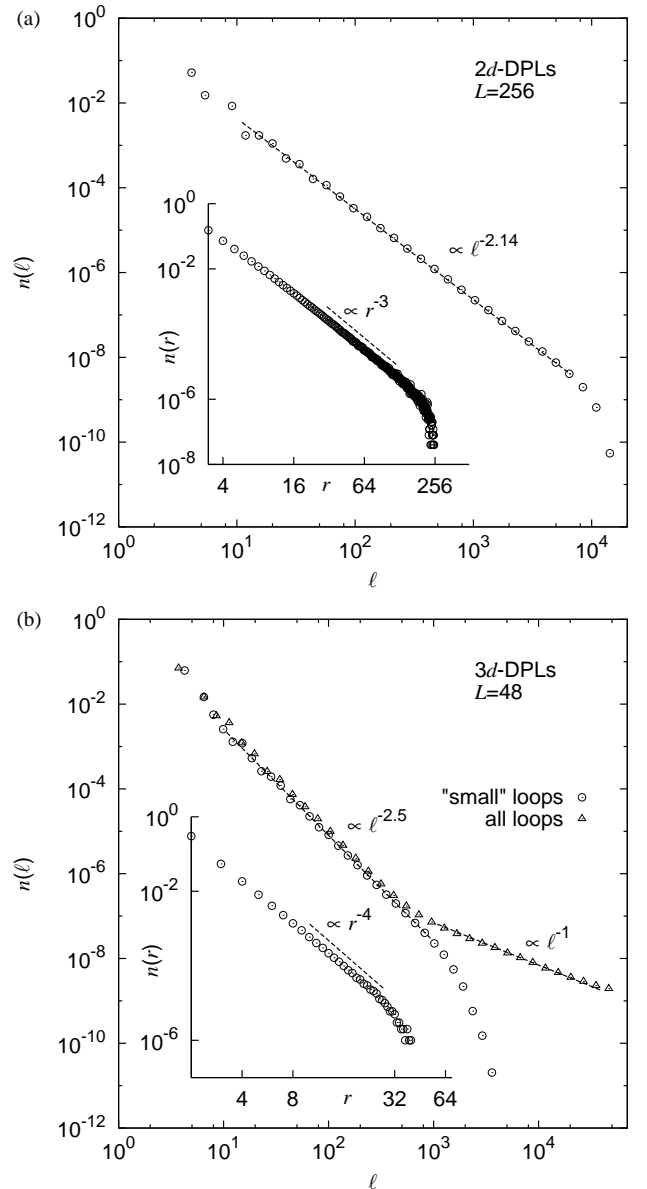


Fig. 5. Results obtained for the number densities $n(\cdot)$ for loops of length ℓ and roughness r . The main plots show the number density $n(\ell)$ of loops with length ℓ (using logarithmic binning) and the inset illustrates the scaling of the number density $n(r)$ of loops with roughness r . (a) Data obtained for DPLs on the $2d$ square lattice, (b) data for DPLs on the $3d$ simple cubic lattice.

stemming from loops with spanning indices $j = 0, 1$ and 2 . Loops with $j = 0$ contribute to the shortest loops, $j = 2$ the largest loops and $j = 1/j = 2$ contribute to the bulk of intermediate size loops.

Scaling of the loop area in $2d$: For the $2d$ setups we can further associate a *cluster* with each loop. Such a cluster simply consists of the elementary plaquettes enclosed by a loop (for a square lattice, an elementary plaquette con-

sists of a unit square bordered by 4 lattice edges). Consequently, the loop forms the perimeter of its associated cluster. The basic observable related to a cluster is its area (or similarly its volume) $A_{\mathcal{L}}$, measured by the number of elementary plaquettes that comprise the cluster. To support intuition, the exemplary loop configuration $\mathcal{C} = \{\mathcal{L}_1, \mathcal{L}_2\}$ shown in Fig. 2(d) features two clusters with perimeter $\ell_1=8, \ell_2=4$ and area $A_{\mathcal{L}_1}=3, A_{\mathcal{L}_2}=1$.

As introduced earlier, the spanning length R is a typical lengthscale that characterizes an individual loop, and henceforth characterizes also the associated cluster. The area of the clusters is expected to scale as $A_{\mathcal{L}} \sim R^{d_v}$, where d_v signifies the fractal dimension of the cluster area (or volume). For 2d-sq DPLs we find $\langle A_{\mathcal{L}} \rangle \sim R^{1.997(4)}$ (2d-hy DPLs: $d_v = 2.01(1)$; 2d-sq FPLs: $d_v = 1.99(1)$), indicating that the clusters are compact with $d_v = d$. Regarding the fractal scaling of the cluster perimeter ($\ell \sim R^{d_f}$), we might further write $A_{\mathcal{L}} \sim \ell^{d/d_f}$, see Refs. [31,32]. More precise, to account for corrections to scaling we consider a scaling function $\langle A_{\mathcal{L}} \rangle = A_0(\ell + \Delta\ell)^\kappa$ and obtain

	A_0	$\Delta\ell$	κ
DPLs – sq :	0.378(2)	-1.58(6)	1.137(1)
FPLs – sq :	0.323(2)	-0.71(4)	1.135(1)
DPLs – hy :	0.397(9)	-2.2(2)	1.135(4)

Here, since $d_f = d/\kappa$, the scaling exponent κ provides an independent way to estimate the fractal dimension of the loops. In any case, the numerical value of d/κ is in good agreement with the previous estimate of d_f for the respective setup listed in Tab. 1.

Number densities: First, we consider the scaling behavior of the number density $n(R_s)$ of small loops with size R_s . Upon analysis of the 2d and 3d data, we obtain scale invariant expressions of the form $n(R_s) \sim R_s^{-(d+1)}$ (not shown). Arguing as above, it should not matter whether we consider the number density of loops with given spanning length or roughness instead of $n(R_s)$. In this regard, considering only non-spanning loops, we find $n(r) \sim r^{-3.00(3)}$ (2d-sq DPLs) and $n(r) \sim r^{-3.95(6)}$ (3d-sc DPLs), see inset of Figs. 5(a),(b), where in either case the algebraic decay is governed by an exponent in good agreement with $(d+1)$. Note that, if the system of loops is scale invariant, the above scaling behavior can be inferred from a dimensional analysis [7].

Now, the scale invariance of the above number densities, together with the self similar scaling of the loop length, can be used to obtain the scaling assumption $n(\ell) \sim \ell^{-\tau}$ for the number density of loops with length ℓ , see Refs. [7,18,9], defining the exponent $\tau = 1 + d/d_f$. To illustrate this it is useful to consider the number of loops with size from R_s to $R_s + dR_s$, given by $dN = n(R_s) dR_s$. Using the leading order of the relation between the loop length and loop size, i.e. $\ell \sim R_s^{d_f}$ and hence $dR_s \sim \ell^{-1+1/d_f} d\ell$, one can transform dN by a change of variables $R_s \rightarrow \ell$ to yield

$$dN \sim R_s^{-(d+1)} dR_s \sim \ell^{-(1+d/d_f)} d\ell \sim n(\ell) d\ell.$$

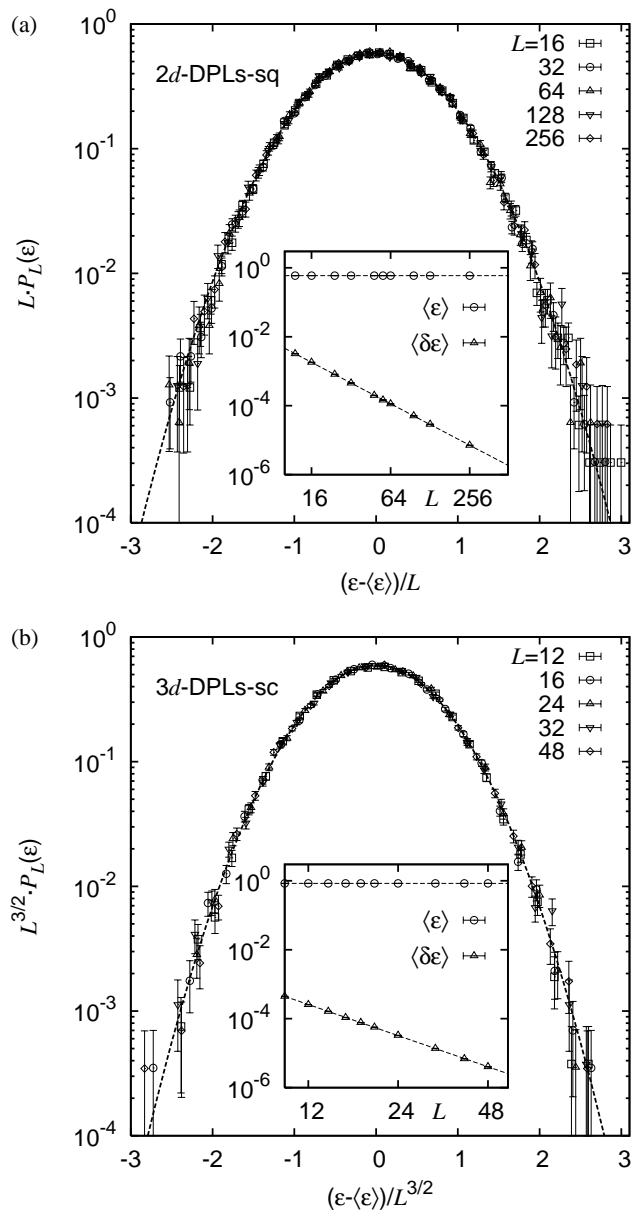


Fig. 6. Results obtained for the pdf $P_L(\epsilon)$ of the configurational energy per lattice site ϵ . (a) Data obtained for DPLs on the 2d square lattice, (b) data for DPLs on the 3d simple cubic lattice. In either case, the shape of $P_L(\epsilon)$ compares well to a Gaussian distribution (indicated by the dashed line). The insets illustrate the average and the instance to instance fluctuation of ϵ as function of the system size L .

The scaling assumption for $n(\ell)$ above fits the data quite well, where, for the setups considered here, we yield the estimates of τ listed in Tab. 1. The data for the 2d-sq and 3d-sc DPLs is shown in Figs. 5(a),(b), respectively. Finally, note that the values of τ and d_f listed in Tab. 1 where obtained independently and agree with the scaling relation above within errorbars.

Note that, for the $3d$ -sc DPL setup, if one considers all loops (not only the non-spanning loops) in order to compute the distribution $n(\ell)$, one finds a crossover to the scaling behavior $n(\ell) \sim \ell^{-1}$ in the limit of long loops (i.e. $\ell > 10^3$ for the $3d$ -sc lattice with $L = 48$, see Fig. 5(b)). This behavior is a direct consequence of the periodic boundary conditions that allow for long loops that wind around the lattice, i.e. those loops with a spanning index $j > 0$. Such a crossover behavior was also observed within simulations of other string bearing models [33,34], and, by analytic means, for a simple model of string formation on periodic lattices [19].

3.2 Energetic properties

Scaling of the configurational energy: The disorder averaged total weight $\langle \mathcal{E} \rangle$ of the loop configuration is an extensive quantity for which we found a clear asymptotic scaling that allows us to estimate numerical values for $\langle \epsilon \rangle \equiv \langle |\mathcal{E}| / L^d \rangle$ as listed in Tab. 1. Here, we found no clear-cut deviations from the scaling behavior that might allow for an analysis of corrections to scaling. In this regard, for the smallest $2d$ -sq DPL system considered we found $\epsilon = 0.5965$ ($L = 12$), while for the largest system we obtained $\epsilon = 0.5958$ ($L = 256$). For the $3d$ -sc DPL setup we similarly find $\epsilon = 0.84447$ ($L = 10$) and $\epsilon = 0.84446$ ($L = 48$).

Moreover, the pdf $P_L(\epsilon)$ compares well to a Gaussian distribution, as shown for $2d$ -sq and $3d$ -sc DPLs in Figs. 6(a),(b), respectively. We further analyzed the instance to instance fluctuations $\langle \delta \epsilon \rangle = [\langle \epsilon^2 \rangle - \langle \epsilon \rangle^2]^{1/2}$ (inset of Figs. 6(a),(b)), for which we estimate $\langle \delta \epsilon \rangle = 0.680(4)L^{-0.999(2)}$ ($2d$ -sq DPLs) and $\langle \delta \epsilon \rangle = 0.68(1)L^{-1.504(6)}$ ($3d$ -sc DPLs). We therefore deduce the asymptotic scaling $\langle \delta \epsilon \rangle \sim L^{-d/2}$. Note that in terms of the extensive configurational energy \mathcal{E} , the latter reads $\langle \delta \mathcal{E} \rangle \sim L^{d/2}$ and is thus in agreement with the result for finite dimensional spin glasses [35]. As evident from Fig. 6, the data sets for different system sizes show a nice data collapse if rescaled according to $P_L(\epsilon) = L^{-d/2} p_1[(\epsilon - \langle \epsilon \rangle) / L^{d/2}]$.

Considering DPLs for $2d$ square and honeycomb lattice graphs, one might speculate whether the respective estimates of $\langle \epsilon \rangle$ reduce to a unique value, apart from purely geometric factors. In this regard, assuming that ϵ depends on the fraction of occupied lattice sites ρ_{cov} as well as the coordination number z that characterizes the particular lattice geometry ($2d$ -sq: $z = 4$; $2d$ -hy: $z = 3$), we find that the simple expression $\langle \epsilon \rangle = 0.182 \cdot z \cdot \rho_{\text{cov}}$ fits the respective values of $\langle \epsilon \rangle$ (listed in Tab. 1) quite well.

Scaling properties of the loop weight: Further, we investigated the scaling of the average loop weight $\langle \omega_{\mathcal{L}} \rangle$ as function of the loop spanning length R by considering the full ensemble of loops collected at the largest system size simulated. In either case we find a good fit to the scaling form $\langle \omega_{\mathcal{L}} \rangle \sim R^\alpha (1 + cR^{-\beta})$, where we yield the exponents $\alpha = 1.759(7)$ ($2.05(7)$) and $\beta = 0.84(4)$ ($0.58(7)$) for $2d$ -sq ($3d$ -sc) DPLs (results for the $3d$ -sc

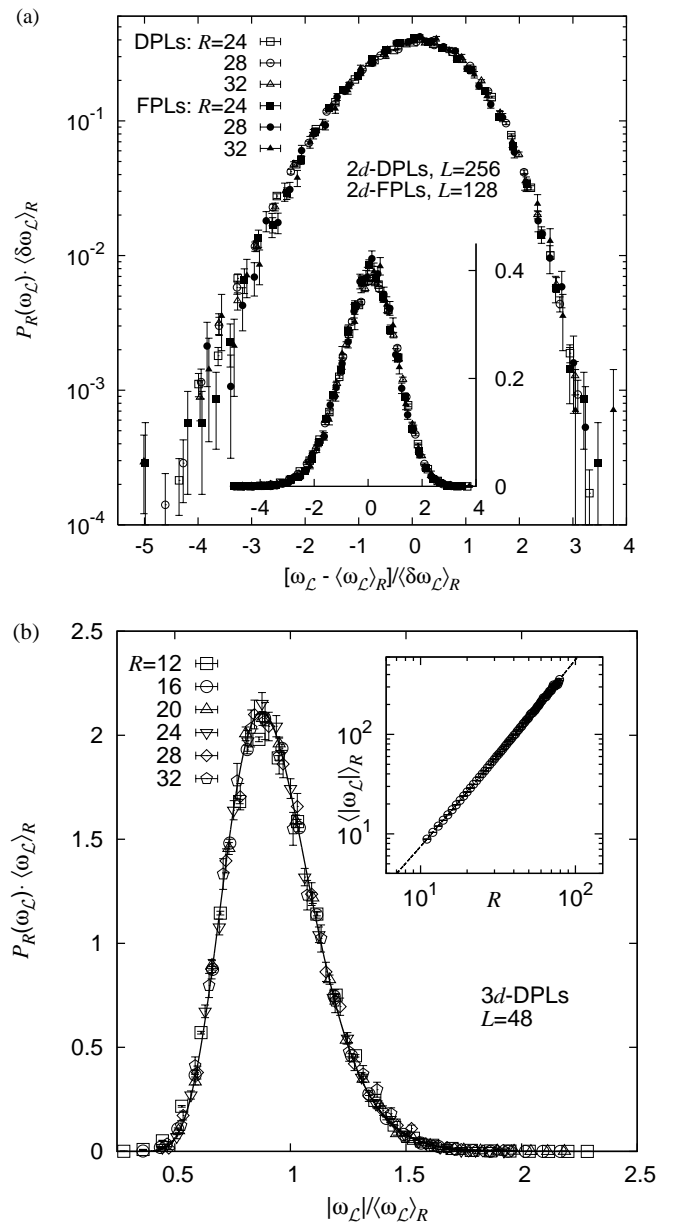


Fig. 7. Scaling of the probability density function (pdf) $P_R(\omega_{\mathcal{L}})$ for the loop weight $\omega_{\mathcal{L}}$ of loops with spanning length R . (a) the main plot shows the scaling of the pdf for $2d$ DPLs and FPLs on a semi-logarithmic scale, while the inset shows the same data on a linear scale. (b) scaling behavior of the pdf for $3d$ DPLs, where the scaling function $\tilde{p}_2[|\omega_{\mathcal{L}}| / \langle \omega_{\mathcal{L}} \rangle_R]$ (solid line) compares well to a log-normal distribution function as discussed in the text. The inset shows the scaling of the average loop weight as function of the spanning length R .

data are shown in the inset of Fig. 7(b)). For the $2d$ -sq FPL setup and considering a similar scaling expression, we yield $\alpha = 1.75(2)$ and $\beta = 0.87(17)$ (here, a more basic scaling function yields $\langle \omega_{\mathcal{L}} \rangle \sim (R + 1.3(2))^{1.74(1)}$). Note that a scaling according to the expression above, together

with the numerical values of the respective exponents, indicates that $\langle\omega_{\mathcal{L}}\rangle\sim\ell$. Moreover, the root mean square deviation $\langle\delta\omega_{\mathcal{L}}\rangle=[\langle\omega_{\mathcal{L}}^2\rangle-\langle\omega_{\mathcal{L}}\rangle^2]^{1/2}$ exhibits the same asymptotic scaling as the average loop weight, i.e. $\langle\delta\omega_{\mathcal{L}}\rangle\sim R^\alpha$ for sufficiently large values of R . However, for small values of R there are also deviations from a pure power law scaling that might be accounted for by using a scaling expression of the form $\langle\delta\omega_{\mathcal{L}}\rangle\sim(R+\Delta R)^\alpha$. E.g., for $2d$ -sq DPLs (FPLs) we find $\Delta R=4(1)$ (12.5(3)) and $\alpha'=1.75(2)$ (1.77(2)).

In either case, the pdf $P_R(\omega_{\mathcal{L}})$ of the loop weight for loops of different spanning length R exhibits the scaling behavior $P_R(\omega_{\mathcal{L}})\sim\langle\delta\omega_{\mathcal{L}}\rangle_R^{-1}p_2[(\omega_{\mathcal{L}}-\langle\omega_{\mathcal{L}}\rangle_R)/\langle\delta\omega_{\mathcal{L}}\rangle_R]$. Comparing $2d$ -sq DPLs and FPLs, we find that both setups appear to have the same scaling function $p_2[\cdot]$, i.e. after rescaling both data sets displayed in Fig. 7(a) fall onto a unique mastercurve.

For the $3d$ -sc case, we observe that $\langle\omega_{\mathcal{L}}\rangle_R\sim\langle\delta\omega_{\mathcal{L}}\rangle_R$ already for small values of R . Thus, the data fits a slightly simpler scaling assumption, i.e. $P_R(\omega_{\mathcal{L}})=\langle\omega_{\mathcal{L}}\rangle_R^{-1}\tilde{p}_2[|\omega_{\mathcal{L}}|/\langle\omega_{\mathcal{L}}\rangle_R]$, where the scaling function $\tilde{p}_2[x]$ can further be parameterized by the log-normal distribution function $\tilde{p}_2[x]=\exp[-(\log(x)-\mu)^2/(2\sigma^2)]/(x\sigma\sqrt{2\pi})$ with parameters $\mu=-0.089(1)$ and $\sigma=0.211(1)$, illustrated by the solid line in Fig. 7(b).

4 Conclusions

In the presented study, we performed simulations to characterize geometric and energetic properties of densely and fully packed configurations of loops in the negative-weight percolation model. Therefore, we considered a Gaussian distribution of the edge weights and $2d$ square/honeycomb and $3d$ simple cubic lattice graphs. Further, so as to obtain configurations of minimum weight loops, we used a mapping of the NWP model to a combinatorial optimization problem that can be solved by means of exact algorithms. In subsequent FSS analyses we observed that the scaling behavior of observables is best represented by considering scaling expressions that also account for small power law corrections.

Regarding the $2d$ setups, we found that the configurations of loops for both, DPLs and FPLs, are characterized by the same values of the geometric scaling exponents d_f and τ . Moreover, the numerical value of d_f found here coincides with the one measured for the smart kinetic walk (SKW) [36]. A loop-forming version of the SKW in two dimensions traces out the external perimeter of critical percolation clusters and was also used to model ring polymers at the θ' -point (which presumably is in the same universality class as the θ -point) on the honeycomb lattice [37]. Also, it compares well to experimental results on the scaling of the radius of gyration of $2d$ polymeric chains [38]. In that study, polymethylmetacrylate (PMMA) was spread onto an air-water interface at 16.5°C that acted as a θ -solvent for the respective polymer material. Further, the exponents d_f and τ agree with those measured for fully packed loops on two discrete interface models

termed “random manifold” and “random elastic medium” [23]. Finally, upon analysis of the pdfs that describe the scaling of the loop length as well as the loop weight, we found a universal behavior regarding the different $2d$ setups considered.

For the $3d$ setup, we observed two phases of loops containing “small” non-spanning loops and “large” spanning loops, respectively. Both phases are characterized by different geometric properties. Such a phenomenon was also observed for other string-bearing models, as e.g. cosmic string networks [33,34] or more general models of string formation on periodic lattices [19,18]. Regarding the small loop phase we conclude with a fractal dimension $d_f\approx 2.01(4)$. As discussed earlier, this scaling exponent indicates that the upper critical dimension for the DPLs takes the value $d_u^{\text{DPL}}=3$. In contrast to this, earlier studies revealed that the upper critical dimension of the NWP model at the critical point where percolating loops first appear in the limit of large system sizes is $d_u=6$ [22]. As for usual self-avoiding lattice curves for $d\geq d_u^{\text{DPL}}$, one can further expect to find $d_f=2$. This we confirmed for DPLs on $4d$ hypercubic lattice graphs, where we obtained the estimate $d_f=2.00(5)$. Further, the large loop phase is a direct consequence of the periodic boundary conditions of the simulated systems. Upon analysis, we found that approximately 90% of the sites on the $3d$ simple cubic lattice are visited by loops and large loops comprise about 91% of the loop segments on the lattice. Hence, these loops fill extensive parts of the “simulation box” and are strongly affected by the finite size of the accessible volume. Within the large loop phase we found evidence that the scaling properties of the loops further depend on their precise topology.

Finally, note that the algorithmic procedure presented in section 2 is not limited to a particular disorder distribution or lattice setup and thus allows for the analysis of configurations of DPLs and FPLs for a multitude of lattice geometries and lattice dimensions.

OM acknowledges financial support from the VolkswagenStiftung (Germany) within the program “Nachwuchsgruppen an Universitäten”. The simulations were performed at the GOLEM I cluster for scientific computing at the University of Oldenburg (Germany).

References

1. M. Kardar and Y. C. Zhang. Scaling of Directed Polymers in Random Media. *Phys. Rev. Lett.*, 58:2087, 1987.
2. B. Derrida. Directed polymers in a random medium. *Physica A*, 163:71, 1990.
3. P. Grassberger. Recursive sampling of random walks: self-avoiding walks in disordered media. *J. Phys. A*, 26:1023, 1993.
4. S. V. Buldyrev, S. Havlin, and H. E. Stanley. Optimal paths in strong and weak disorder: A unified approach. *Phys. Rev. E*, 73, 2006.
5. F. O. Pfeiffer and H. Rieger. Superconductor-to-normal phase transition in a vortex glass model: numerical evi-

- dence for a new percolation universality class. *J. Phys.: Condens. Matter*, 14:2361, 2002.
6. F. O. Pfeiffer and H. Rieger. Critical properties of loop percolation models with optimization constraints. *Phys. Rev. E*, 67(5):056113, 2003.
 7. T. Vachaspati and A. Vilenkin. Formation and evolution of cosmic strings. *Phys. Rev. D*, 30(10):2036, 1984.
 8. R. J. Scherrer and J. A. Frieman. Cosmic strings as random walks. *Phys. Rev. D*, 33, 1986.
 9. H. Hindmarsch and K. Strobl. Statistical properties of strings. *Nucl. Phys. B*, 437:471, 1995.
 10. M. Cieplak, A. Maritan, and J. R. Banavar. Optimal paths and domain walls in the strong disorder limit. *Phys. Rev. Lett.*, 72:2320, 1994.
 11. O. Melchert and A. K. Hartmann. Fractal dimension of domain walls in two-dimensional Ising spin glasses. *Phys. Rev. B*, 76:174411, 2007.
 12. K. Schwarz, A. Karrenbauer, G. Schehr, and H. Rieger. Domain walls and chaos in the disordered SOS model. *J. Stat. Mech.*, 2009:P08022, 2009.
 13. N. Schwartz, A. L. Nazaryev, and S. Havlin. Optimal path in two and three dimensions. *Phys. Rev. E*, 58:7642, 1998.
 14. Heiko Rieger. Polynomial combinatorial optimization methods for analysing the ground states of disordered systems. *J. Phys. A*, 36(43), 2003.
 15. A. K. Hartmann. Domain walls, droplets and barriers in two-dimensional Ising spin glasses. In Janke W, editor, *Rugged Free Energy Landscapes*, pages 67 – 106, Berlin, 2007. Springer.
 16. D. Stauffer. Scaling theory of percolation clusters. *Phys. Rep.*, 54(1):1–45, 1979.
 17. D. Stauffer and A. Aharony. *Introduction to Percolation Theory*. Taylor and Francis, London, 1994.
 18. A. M. Allega, L. A. Fernández, and A. Tarancón. Configurational statistics of strings, fractals and polymer physics. *Nucl. Phys. B*, 332:760, 1990.
 19. D. Austin, E. J. Copeland, and R. J. Rivers. Statistical mechanics of strings on periodic lattices. *Phys. Rev. D*, 49:4089, 1994.
 20. O. Melchert and A. K. Hartmann. Negative-weight percolation. *New. J. Phys.*, 10:043039, 2008.
 21. L. Apolo, O. Melchert, and A. K. Hartmann. Phase transitions in diluted negative-weight percolation models. *Phys. Rev. E*, 79:031103, 2009.
 22. O. Melchert, L. Apolo, and A. K. Hartmann. Upper critical dimension of the negative-weight percolation problem. *Phys. Rev. E*, 81(5):051108, 2010.
 23. C. Zeng, J. Kondev, D. McNamara, and A. A. Middleton. Statistical Topography of Glassy Interfaces. *Phys. Rev. Lett.*, 80(1), 1998.
 24. R. K. Ahuja, T. L. Magnanti, and J. B. Orlin. *Network Flows: Theory, Algorithms, and Applications*. Prentice Hall, 1993.
 25. W. Cook and A. Rohe. Computing minimum-weight perfect matchings. *INFORMS J. Computing*, 11:138–148, 1999.
 26. A. K. Hartmann and H. Rieger. *Optimization Algorithms in Physics*. Wiley-VCH, Weinheim, 2001.
 27. O. Melchert. *PhD thesis*. not published, 2009.
 28. A. K. Hartmann. *Practical Guide to Computer Simulations*. World Scientific, Singapore, 2009.
 29. For the calculation of minimum-weighted perfect matchings we use Cook and Rohes blossom4 extension to the Concorde library.
 30. M. Camarda, F. Siringo, R. Pucci, A. Sudbø, and J. Hove. Methods to determine the Hausdorff dimension of vortex loops in the three-dimensional XY model. *Phys. Rev. B*, 74(10):104507, 2006.
 31. S. Leibler, R. R. P. Singh, and M. E. Fisher. Thermodynamic behavior of two-dimensional vesicles. *Phys. Rev. Lett.*, 59:1989, 1987.
 32. B. Duplantier. Exact fractal area of two-dimensional vesicles. *Phys. Rev. Lett.*, 64(4):493, 1990.
 33. A. M. Allega, L. A. Fernández, and A. Tarancón. New regimes in the initial cosmic string network. *Phys. Lett. B*, 227:347, 1989.
 34. A. M. Allega. Scaling in a string network. *Phys. Rev. D*, 40:1017, 1989.
 35. J. Wehr and M. Aizenman. Fluctuations of extensive functions of quenched random couplings. *J. Stat. Phys.*, 60:287, 1990.
 36. A. Weinrib and S. A. Trugman. A new kinetic walk and percolation perimeters. *Phys. Rev. B*, 31:2993, 1985.
 37. A. Coniglio, N. Jan, I. Majid, and H. E. Stanley. Conformation of a polymer chain at the theta' point: Connection to the external perimeter of a percolation cluster. *Phys. Rev. B*, 35:3617, 1987.
 38. R. Vilanove and F. Rondelez. Scaling Description of Two-Dimensional Chain Conformations in Polymer Monolayers. *Phys. Rev. Lett.*, 45(18):1502, 1980.